Overexpression of peroxisomal testis-specific 1 protein induces germ cell apoptosis and leads to infertility in male mice

Karina Kaczmarek[a], Maja Studencka[a], Andreas Meinhardt[b], Krzysztof Wieczerzak[a], Sven Thoms[c], Wolfgang Engel[a], and Pawel Grzmil[a,d]

[a]Institute of Human Genetics, Georg-August-University of Göttingen, 37073 Göttingen, Germany; [b]Department of Anatomy and Cell Biology, Justus-Liebig-University Giessen, 35385 Giessen, Germany; [c]Department of Pediatrics and Pediatric Neurology, University of Göttingen, 37075 Göttingen, Germany; [d]Department of Genetics and Evolution, Institute of Zoology, Jagiellonian University, 30-060 Cracow, Poland

ABSTRACT **Peroxisomal testis-specific 1 gene (*Pxt1*) is the only male germ cell–specific gene that encodes a peroxisomal protein known to date. To elucidate the role of *Pxt1* in spermatogenesis, we generated transgenic mice expressing a c-MYC-PXT1 fusion protein under the control of the *PGK2* promoter. Overexpression of *Pxt1* resulted in induction of male germ cells' apoptosis mainly in primary spermatocytes, finally leading to male infertility. This prompted us to analyze the proapoptotic character of mouse PXT1, which harbors a BH3-like domain in the N-terminal part. In different cell lines, the overexpression of PXT1 also resulted in a dramatic increase of apoptosis, whereas the deletion of the BH3-like domain significantly reduced cell death events, thereby confirming that the domain is functional and essential for the proapoptotic activity of PXT1. Moreover, we demonstrated that PXT1 interacts with apoptosis regulator BAT3, which, if overexpressed, can protect cells from the PXT1-induced apoptosis. The PXT1-BAT3 association leads to PXT1 relocation from the cytoplasm to the nucleus. In summary, we demonstrated that PXT1 induces apoptosis via the BH3-like domain and that this process is inhibited by BAT3.**

Monitoring Editor
Kunxin Luo
University of California, Berkeley

Received: Dec 1, 2009
Revised: Mar 18, 2011
Accepted: Mar 22, 2011

INTRODUCTION

Programmed cell death (apoptosis) is an active, highly regulated biological process that enables maintenance of tissue homeostasis by elimination of aged, overproduced, or dysfunctional cells. Apoptotic loss of germ cells during testicular development is very common in both normal and pathological conditions (Hikim *et al.*, 1998), but the mechanisms and genes underlying this important event in the male gonad still remain unclear. One candidate gene predominantly expressed in the testis that is involved in apoptosis is HLA-B-associated transcript 3 (*Bat3*, also known as *Scythe* or *Bag6*) (Wang and Liew 1994; Ozaki *et al.*, 1999). BAT3 is a member of the BCL-2-associated athanogene (BAG) family of proteins that, aside from a C-terminal BAG domain, contains two C-terminal nuclear localization signals, central polyproline- and glutamine-rich regions, zinc-finger-like motif, as well as an N-terminal ubiquitin-like domain (Banerji *et al.*, 1990; Manchen and Hubberstey 2001). It has been demonstrated that BAT3 interacts with the *Drosophila* proapoptotic protein reaper and modulates reaper-induced apoptosis. In addition, the interaction of BAT3 with many other apoptotic regulators, such as p53, NCR3, AIFM1, and PBF, has been reported (Pogge von Strandmann *et al.*, 2007; Sasaki *et al.*, 2007; Desmots *et al.*, 2008; Tsukahara *et al.*, 2009). Interestingly, the targeted disruption of *Bat3* in mice induces apoptosis of meiotic germ cells, resulting in complete male infertility (Sasaki *et al.*, 2008). The authors have demonstrated that stabilization of HSPA1B (also known as HSP70–2) by BAT3 is crucial for proper function of HSPA1B during spermatogenesis.

To date, the peroxisomal testis specific 1 (*Pxt1*) gene is the only known gene that encodes a male germ cell–specific peroxisomal protein (Grzmil *et al.*, 2007). The expression of *Pxt1* is developmentally regulated during spermatogenesis, and the

This article was published online ahead of print in MBoC in Press (http://www.molbiolcell.org/cgi/doi/10.1091/mbc.E09-12-0993) on April 1, 2011.

Address correspondence to: Pawel Grzmil (pawel.grzmil@med.uni-goettingen.de).

Abbreviations used: *Bat3*, HLA-B–associated transcript 3; dsRED, *Discosoma* sp. red fluorescent protein; EGFP, enhanced green fluorescent protein; ORF, open reading frame; *Pxt1*, peroxisomal, testis specific 1.

encoded protein consists of 51 amino acids only. It has been demonstrated previously that PXT1 contains a functional peroxisomal targeting signal type 1 (PTS1) at the C terminus, and the EGFP-PXT1 fusion protein colocalizes with known peroxisomal markers (Grzmil *et al.,* 2007). Peroxisomes are important cellular organelles indispensable for cell survival, and they are ubiquitously present in eukaryotic cells. However, the existence of peroxisomes in male germ cells was questioned for a long time. The first report about the presence of peroxisomes in a spermatogonial cell line was published in 2003 (Luers *et al.,* 2003). Later, peroxisomes were detected in spermatogonia of mouse testis (Huyghe *et al.,* 2006a; Luers *et al.,* 2006). Recently, using antibodies against different peroxisomal marker proteins, Nenicu *et al*. (2007) have demonstrated peroxisomes in all stages of spermatogenesis, except mature spermatozoa. There are many mutant mouse models in which peroxisome-associated spermatogenesis defects have been observed. Among them, targeted disruption of the acyl-coenzyme A oxidase 1 (*Acox1*) gene results in a remarkable reduction of Leydig cells, hypospermatogenesis, and male infertility (Fan *et al.,* 1996). Deficiency of glyceronephosphate *O*-acyltransferase (*Gnpat*) also leads to testicular atrophy and male infertility (Rodemer *et al.,* 2003). The analysis of knockout mice lacking the peroxisomal protein hydroxysteroid (17-beta) dehydrogenase 4 (HSD17B4; also known as multifunctional protein 2, MFP-2) has revealed that homozygous male mutants exhibit a strongly reduced fertility (Baes *et al.,* 2000; Huyghe *et al.,* 2006a). Although these findings have confirmed the general relevance of peroxisomes for proper spermatogenesis, the biological function of these organelles in the testis still remains poorly understood.

To further elucidate the function of *Pxt1* and peroxisomes in mouse testis, we have generated transgenic mice with male germ cell–specific overexpression of PXT1. In the present work, we show that overexpression of PXT1 induces apoptosis, resulting in male infertility. Moreover, we demonstrate that PXT1 interacts with BAT3 and that BAT3 can inhibit the proapoptotic activity of PXT1 in transiently transfected cell lines.

RESULTS

Generation of the c-myc-Pxt1 transgenic line

The male germ cell–specific expression of *Pxt1* (Grzmil *et al.,* 2007) prompted us to investigate the in vivo function of this gene during spermatogenesis. For this purpose the c-myc-Pxt1 transgenic construct (Figure 1A) expressing *c-myc-Pxt1* fusion transcript under the control of the human *PGK2* promoter was generated. Downstream of the *Pxt1* ORF, the 3′ untranslated region (UTR) of human growth hormone 1 (*GH1*) and SV40 poly(A) sequence were located in order to ensure the proper posttranscriptional proceeding of the transgenic mRNA. The transgenic cassette was microinjected into the pronuclei of fertilized FVB/N mouse eggs, and founder mice were detected by PCR using genomic DNA and the following transgenic construct–specific primers: gen_hPGK2_F1, gen_Pxt1ex.2–3_R. As can been seen in Figure 1B, the 674-bp fragment was observed only in founder animals. DNA quality was confirmed with *Tnp2*-specific primers (Figure 1B). Initially, four transgenic male founders were identified, and each of them was mated with two wild-type FVB/N females to establish the transgenic line. After a 3-mo breeding period, no pregnancy could be observed, suggesting infertility of the male founders. We have also identified a female founder that was fertile and able to transmit the transgene to its progeny. The female founder was mated with wild-type FVB/N male, and using the PCR genotyping, we detected the transgenic animals in the F_1 generation and established the transgenic line.

Testis-specific expression of the c-myc-Pxt1 transgene

To confirm that the 1.4-kb region of *PGK2* promoter properly conferred the expression of *c-myc-Pxt1* to the testis, total RNA was isolated from various tissues of adult transgenic males. Northern blot experiment with the *Pxt1*-specific probe, which recognizes the full length of *Pxt1* ORF, revealed that the expected 1.2-kb band representing the endogenous *Pxt1* mRNAs could be observed in both wild-type and transgenic testes. In addition, the same probe detected the 0.8-kb band corresponding to the *c-myc-Pxt1* fusion transcripts exclusively in transgenic testis (Figure 1C, top). As can be seen in middle panel of Figure 1C, the 0.8-kb band was also identified in the transgenic testis when membrane was hybridized with the *c-myc* tag–specific probe. The integrity of all RNA samples was assessed by rehybridization of the blots with *Eef1a1* cDNA probe (Figure 1C, bottom). To confirm the Northern blot results, a more sensitive RT-PCR method was used. Likewise, the testis-specific expression of the c-myc-Pxt1 transgene was confirmed (Figure 1D). To analyze the expression of the c-myc-Pxt1 transgene during spermatogenesis, RT-PCR was performed with RNA from testes of transgenic mice at different postnatal ages. A first weak signal could be observed in the testis at 10 d postpartum (dpp), whereas a stronger band was obtained at 17 and 19 dpp (Figure 1E). To check for DNA contamination in RNA samples, the reaction without reverse transcriptase (−RT) was performed (Figure 1, D and E). The cDNA quality was proven with *Hprt1*-specific primers (Figure 1, D and E, lower panels). Next the expression of c-MYC-PXT1 fusion protein was evaluated by Western blot using anti–myc tag antibody. The expected 17-kDa band corresponding to the size predicted for c-MYC-PXT1 fusion protein was detected in the testes of transgenic mice but not in the epididymis of transgenic mice or analyzed wild-type tissues (Figure 1F). Protein quality and integrity were verified using anti–β-actin (ACTB) antibody (Figure 1F, bottom). We have previously demonstrated that EGFP-PXT1 fusion protein colocalized with peroxisomal marker proteins in transiently transfected cells (Grzmil *et al.* 2007). To determine whether the c-MYC-PXT1 fusion protein also colocalizes with peroxisomal markers in germ cells, the transgenic and wild-type testis sections were innumostained with anti–myc tag and anti–PMP70 antibodies. The c-MYC-PXT1 fusion protein could be detected within the cytosol of transgenic pachytene spermatocytes (Figure 1G) but not in the wild type (Figure 1K). The PMP70 was detected in both transgenic and wild-type testes (Figure 1, H and L). The strongest expression of PMP70 was observed in the outer layer of the seminiferous epithelium, as described previously (Huyghe *et al.,* 2006a), but detectable signals were also observed in cells located more central. In the transgenic testis, the partial colocalization of c-MYC-PXT1 and peroxisomal marker PMP70 was detected (Figure 1, I and J), whereas in the wild-type testis, only the PMP70 protein was detectable (Figure 1, M and N). Moreover, c-MYC-PXT1 colocalized with two additional peroxisomal marker proteins: catalase and PEX13 in the testis (Supplemental Figure 1). Our findings indicated that the c-MYC-PXT1 fusion protein is targeted to peroxisomes in germ cells of transgenic males.

Infertility of the c-myc-Pxt1 transgenic male mice

As mentioned, a female founder was used to generate the transgenic line, because all four tested male founders were infertile. To examine the fertility of male progeny of the female founder, three males were mated each with two wild-type females for a period of 3 mo. During this time, the females were monitored daily for vaginal

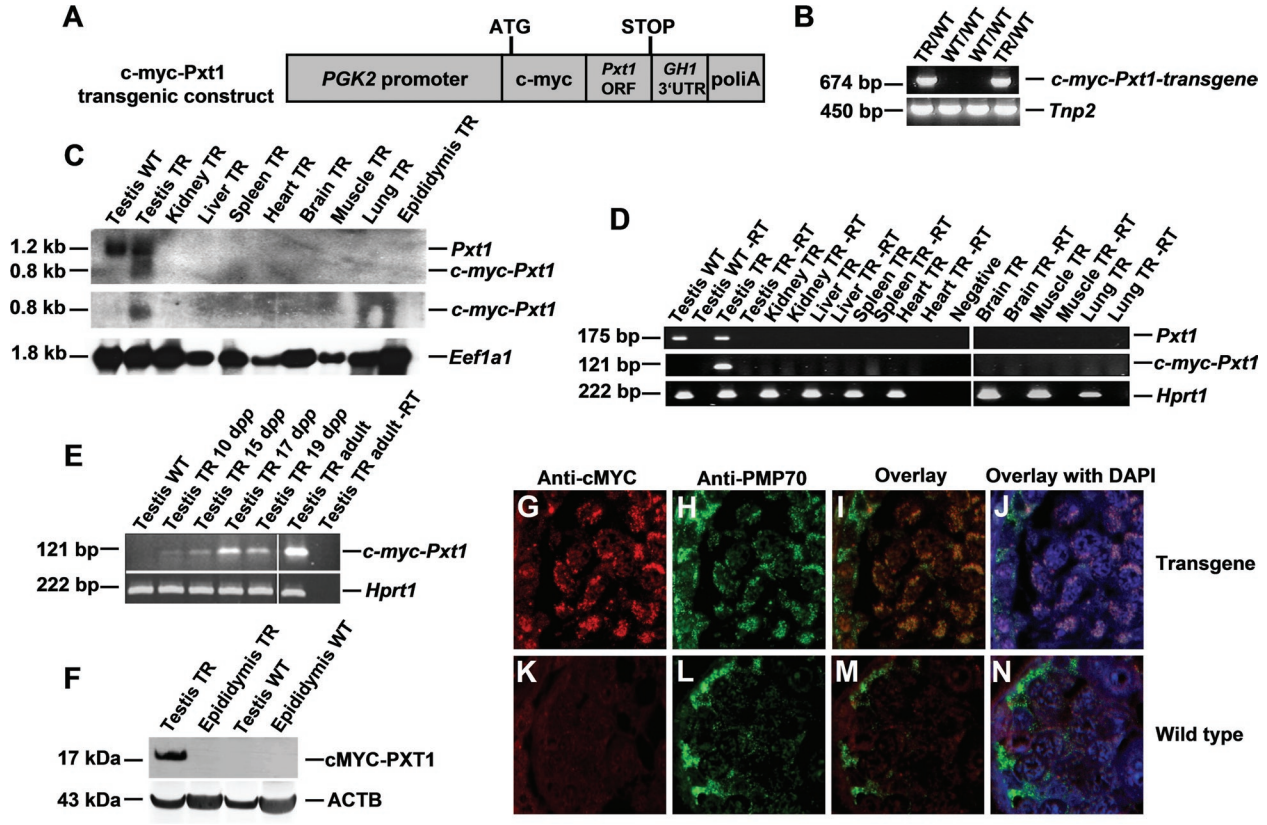

FIGURE 1: Generation and expression analyses of c-myc-Pxt1 transgenic line. (A) Schematic representation of the c-myc-Pxt1 transgenic construct. The construct consists of a 1.4-kb part of the *PGK2* promoter, c-myc-tag, complete ORF of the mouse *Pxt1* gene, 3'UTR of the *GH1* and poly(A) signal of SV40. Start codon (ATG) and stop codon are given. (B) Genotyping PCR of the transgenic founders using transgenic construct-specific primers. A 674-bp product could be observed in transgenic founders (TR/WT) but not in wild-type (WT/WT) animals. DNA quality was verified with *Tnp2*-specific primers (bottom). (C) Northern blot analysis of the c-myc-Pxt1 transgene expression in different organs of transgenic males. Using the *Pxt1*-specific probe, we demonstrated a 1.2-kb band, representing the endogenous *Pxt1* in the testis of wild type (WT) and transgenic (TR) and a 0.8-kb band corresponding to the *c-myc-Pxt1* transcript in TR testis (top). As expected, the *c-myc*–specific probe detected the 0.8-kb band, representing *c-myc-Pxt1* mRNA, only in the transgenic testis (middle). RNA quality and integrity was checked using the *Eef1a1*-specific probe (bottom). (D) To confirm the testis-specific expression of the c-myc-Pxt1 transgene, the RT-PCR analysis was performed. The *Pxt1*-specific primers amplified the 175-bp fragment in testis of WT and TR males, whereas the c-myc-Pxt1 construct–specific primers amplified the 121-bp product only in the testis of transgenic male. (E) To analyze the c-myc-Pxt1 transgene expression during spermatogenesis, RT-PCR was performed with testicular RNA of transgenic mice at different postnatal ages. Weak signal was observed in testis at 10 and 15 dpp, whereas a stronger band was obtained at 17 and 19 dpp. The cDNA quality in both RT-PCR reactions was proven using the *Hprt*-specific primers amplifying 222-bp product in all analyzed cDNA samples (D, E, bottom). To exclude any genomic DNA contamination, negative controls without reverse transcriptase were performed (−RT) (D, E). (F) Western blot analysis using anti–myc tag antibody demonstrated the expected 17 kDa c-MYC-PXT1 fusion protein in testis of TR but not in WT animals. To check the protein quality, anti–β-actin antibody (ACTB) was used. In the testicular sections of transgenic mice, anti–myc tag antibody detected the c-MYC-PXT1 fusion protein in the seminiferous tubuli, mainly in primary spermatocytes (G). Peroxisomal PMP70 protein was detected by immonostaining with specific antibody (H and L), and the colocalization of c-MYC-PXT1 fusion protein and the PMP70 was demonstrated in transgenic testis (I and J). Negative immunostaining on WT testis confirmed the specificity of the anti–myc tag antibody (K, M, and N).

plugs (VPs). Although females were positive for VPs (indicating mating), none of them became pregnant. No spermatozoa could be found in the uterus and oviduct of VP-positive females. To evaluate the cause of male infertility in the c-myc-Pxt1 transgenic line, a morphological and histological examination of the male reproductive organs was performed. Transgenic males at 103 dpp demonstrated testicular atrophy (Figure 2A), and the histological analysis revealed arrest of spermatogenesis at the level of pachytene spermatocytes (Figure 2B). Remarkably, only very few degenerating round spermatids and no elongated spermatids were found. The testis displayed massive vacuolization of the seminiferous epithelium, sloughing of immature germ cells into the lumen, and formation of numerous multinucleated giant cells. It should be noted that the range of observed abnormalities varied between tubules, but the epididymal lumen contained numerous immature germ cells and multinucleated giant cells but no or very few spermatozoa (Figure 2C). The phenotype of transgenic males became even more severe with age, and at 151 dpp, complete depletion of germ cells resulting in a Sertoli cell–only (SCO) phenotype was evident (Figure 2D). However, the expression of the c-myc-Pxt1 transgene was weak at 10 dpp (Figure 1E); when spermatogonia are present in the testis (Silver, 1995) in older animals, the accumulation of c-MYC-PXT1

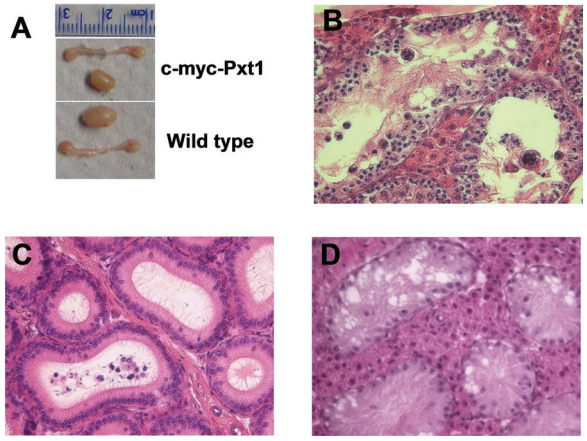

FIGURE 2: Overexpression of c-myc-Pxt1 leads to the degeneration of the germinal epithelium. (A) Testis of adult transgenic males shows atrophy, whereas epididymides are normal. (B) Histological analysis of atrophic testis revealed a prominent degeneration of germ cells in adult animals (103 dpp), especially at the primary spermatocyte stage. Strong vacuolization of the epithelium, immature germ cells in lumen and giant cells could be observed. (C) In epididymides of transgenic animals, very few (or no) spermatozoa were found and often round spermatids and multinucleated giant cells were present. (D) The testis section of transgenic male at 151 dpp shows an SCO phenotype.

fusion protein could reach a toxic level and result in SCO. Stronger expression was observed at 17 dpp (Figure 1E), and the c-MYC-PXT1 fusion protein could first be detected in primary spermatocytes (Figure 1, G, I, and J). Accordingly, to elucidate the defective stage of spermatogenesis in transgenic animals, we analyzed testicular histology at different stages. As demonstrated in Figure 3A, spermatogenesis in mice at 10 dpp appeared normal. Only some histological abnormalities were observed at 16 dpp, before the onset of the meiotic divisions. Some of the pachytene spermatocytes within the seminiferous epithelium exhibited abnormal nuclear morphology, including pyknotic nuclei and a few single nucleated giant cells. In contrast, the histological analysis of older animals revealed that the testicular phenotype at 26 dpp and 38 dpp was almost as severe as that observed in 103-d-old transgenic mice. To investigate whether the progression of seminiferous tubules atrophy caused by overexpression of *Pxt1* is due to increased apoptosis levels, the number of apoptotic cells per tubuli was quantified followed TUNEL staining. This analysis demonstrated that there was no significant increase of apoptosis in transgenic animals at 10 and 16 dpp as compared with wild-type FVB males at the same age (Figure 3, B and C). However, in older animals, a significant increase of apoptosis was observed (Figure 3, B and C). At 30 dpp, the number of apoptotic cells per tubuli was ~13-fold higher in mutant as compared to wild-type testis. Light microscopical analysis following TUNEL assay revealed that pachytene spermatocytes were the predominantly labeled cell type (insets in Figure 3B). In addition, some of the multinucleated giant cells also appeared to undergo apoptosis.

Peroxisomal function is not affected in the testis of c-myc-Pxt1 transgenic males

Disrupted peroxisomal metabolism may result in cell death. Peroxisomes are involved in β-oxidation of very long chain fatty acids (VLCFA) and plasmalogen biosynthesis; thus accumulation of VLCFA and plasmalogen deficiency are typical hallmarks of disturbed peroxisomal metabolism. To rule out the possibility that overexpressed C-MYC-PXT1 fusion protein interferes with peroxisomal import system and thus disturbs normal peroxisomal function, plasmalogen and VLCFA concentration in the testes of transgenic and wild-type mice were measured. Differences in the plasmalogen and VLCFA (C22:0, C24:0, C26:0) concentrations in the testes of c-myc-Pxt1 transgenic animals were not significant as compared with the wild-type control (Table 1). Moreover, the C26/C22 VLCFA concentration ratio differed not significantly between transgenic and control males (0.004 ± 0.0006 vs. 0.0027 ± 0.0019, respectively, p = 0.72), suggesting that PXT1-induced phenotype is not primarily due to altered peroxisomal metabolism.

	Transgene (N = 4) mean ± SD	Wild type (N = 4) mean ± SD	P
Plasmalogens (arbitrary units)			
C16:0	10.02 ± 1.90	8.37 ± 0.98	0.17
C18:0	3.75 ± 1.38	3.35 ± 2.04	0.75
VLCFA (μmol/l)			
C22:0	53.27 ± 9.01	69.07 ± 36.27	0.43
C24:0	25.45 ± 5.60	25.72 ± 13.79	1.0
C26:0	0.21 ± 0.06	0.13 ± 0.06	0.21

Mutant and control males did not differ significantly in palsmalogen and VLCFA concentration. N, number of analyzed animals; P, significance level.

TABLE 1: Plasmalogen and VLCFA (C22:0, C24:0, C26:0) concentration in testes of c-myc-Pxt1 transgenic and FVB wild-type animals.

Murine PXT1 is a proapoptotic BH3-like motif–containing protein

The strongly enhanced apoptosis observed in transgenic males overexpressing *Pxt1*, which was not a consequence of disrupted peroxisomal function, prompted us to more closely analyze the PXT1 protein sequence. An in silico analysis using the Pfam database (http://pfam.sanger.ac.uk/) revealed that the N-terminal fragment of mouse PXT1 contains a putative BH3-like domain (Figure 4A). To investigate the proapoptotic potential of PXT1 protein and verify the functionality of BH3-like domain, we analyzed apoptotic events in HeLa and NIH3T3 cells transiently transfected with Pxt1pQM-Ntag/A and Pxt1ΔBH3pQM-Ntag/A plasmids. As presented in Figure 4B, Pxt1pQM-Ntag/A encodes a full-length PXT1 protein tagged with N-terminal E2 epitope (E2-PXT1), whereas the Pxt1ΔBH3pQM-Ntag/A vector encodes a mutant E2-PXT1 fusion protein with a deletion of the BH3-like motif (E2-PXT1-BH3del). Fluorescence microscopic examination showed that the majority of HeLa cells overexpressing E2-PXT1 exhibited cytomorphological alternations typical for apoptosis, including nuclear fragmentation, cell rounding and shrinkage, plasma membrane blebbing, and apoptotic body formation (Mund *et al.*, 2003; Nozawa *et al.*, 2009) (Figure 4C, top). In contrast, overexpression of the E2-PXT1-BH3del protein had much a weaker effect on the cell viability, and most transfected HeLa cells displayed normal-appearing morphology (Figure 4C, bottom). Quantitative analysis of apoptotic events demonstrated a significant decrease in percentage of E2-PXT1-BH3del–positive cells possessing apoptotic morphology as compared with E2-PXT1–expressing cells (32% ± 1% vs. 77% ± 8%, respectively; p < 0.01; Figure 4C). The control transfection using the Rtn1pQM-Ntag/A construct resulted in a significantly lower percentage of apoptotic cells (6% ± 2%) than the transfections with Pxt1pQM-Ntag/A or Pxt1ΔBH3pQM-Ntag/A (p < 0.01). To confirm

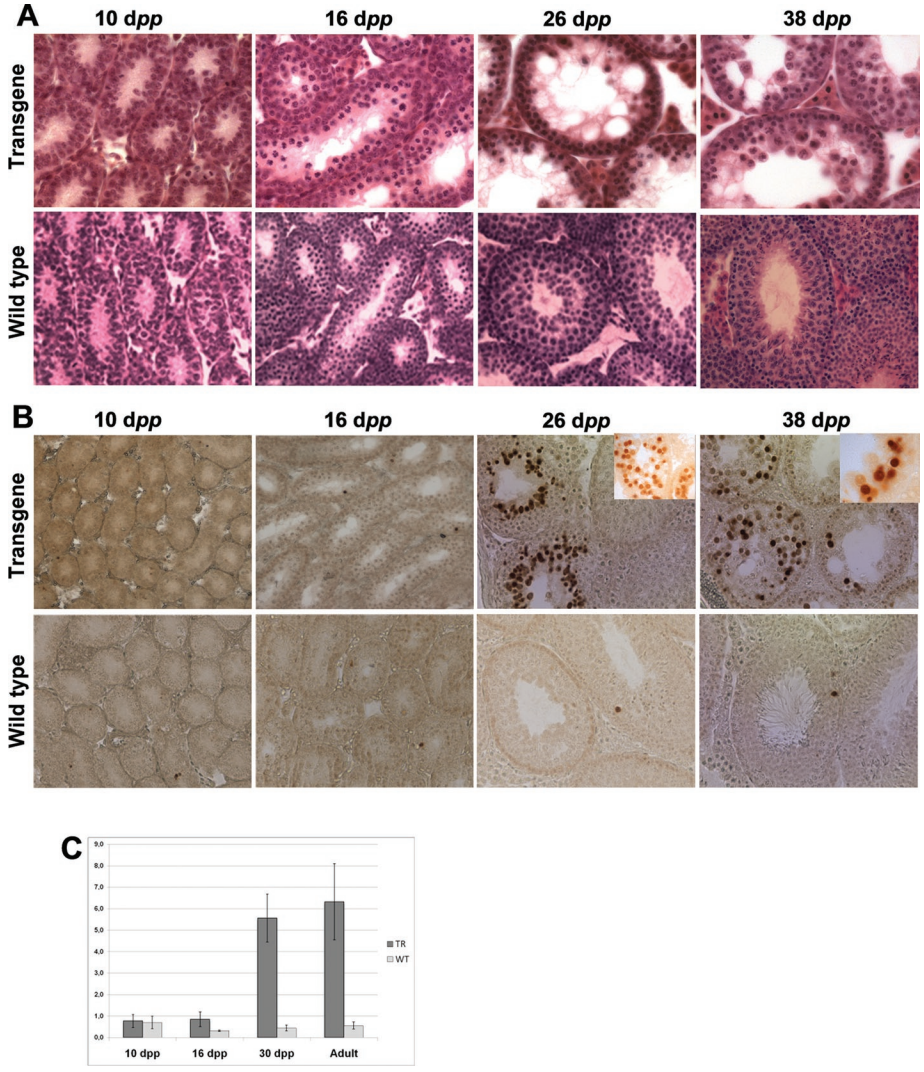

FIGURE 3: Developmental progression of the male germ cells degeneration. (A) At 10 dpp, no obvious changes could be discerned in testes of transgenic males as compared with wild type. The first moderate abnormalities were observed at 16 dpp; however, only a few pachytene spermatocytes exhibited pyknotic nuclei. Massive degeneration was observed at 26 and 38 dpp. (B) To investigate whether the degenerated cells undergo apoptosis, a TUNEL assay was performed. No significant increase in the number of apoptotic cells was observed at 10 and 16 dpp (B and C); in contrast, strong apoptosis induction was observed in older transgenic animals (26, 30, 38 dpp and adult; B and C). Microscopical evaluation revealed that pachytene spermatocytes were predominantly cell type undergoing apoptosis (insets in B).

that the proapoptotic activity of PXT1 was not unique to HeLa cells, we performed similar experiments in the NIH3T3 cell line. The quantitative analysis demonstrated that the kinetics of cell death in NIH3T3 cells were essentially the same as observed in HeLa cells (Supplemental Figure 2).

One of the early characteristics of apoptosis is the externalization of phosphatidylserine (PS) residues on the outer plasma membrane (Casciola-Rosen *et al.*, 1996). Therefore, to further prove the proapoptotic properties of PXT1, we performed an Annexin V Alexa 568 assay of HeLa cells transfected with EGFP-PXT1, EGFP-PXT1-BH3del, and empty EGFP alone (mock). As can be seen in Figure 4D, the majority of EGFP-PXT1–expressing cells were positive for Annexin V and showed typical peripheral staining of the plasma membrane. In contrast, most of the cells expressing EGFP-PXT1-BH3del exhibited normal morphology and no Annexin V staining (Figure 4D, middle panel). The quantification revealed that the percentage of Annexin V–positive cells was approximately three- to fourfold higher in EGFP-PXT1–expressing cells than in EGFP-PXT1-BH3del or EGFP mock cells (75% ± 4% vs. 26% ± 6% or 19% ± 5%, respectively; $p < 0.001$).

PXT1 interacts with BAT3

To gain further insights into the function of PXT1 in the testis, we performed a yeast two-hybrid (Y2H) screen of the mouse testis cDNA library using the full length of murine PXT1 as a bait protein. The screen of total 3.77×10^6 transformants yielded two individual positive clones harboring in-frame sequence of BAT3 protein. The first identified clone (no. 184) contained exons 7–22, and the second (no. 100) exons 7–25 of the *Bat3* cDNA sequence. Direct Y2H assay validated the interaction of PXT1 with BAT3, as can be seen for clone no. 100 in Figure 5A. White yeast colonies growing on medium lacking leucine and tryptophan (−LT) served as cotransformation control, and blue colonies growing in high-stringency conditions (medium lacking leucine, tryptophan, histidine, and adenine, containing X-α-gal (−LTHA+α-gal) indicated PXT1–BAT3 interaction. To confirm the specific and physical binding of PXT1 to BAT3 in mammalian cells, the coimmunoprecipitation (CoIP) assay was performed. HeLa cells were transiently cotransfected with vectors expressing E2-PXT1-BH3del (6 kDa) and c-MYC-BAT3 (101 kDa) fusion proteins. We intentionally used the plasmid encoding PXT1 protein lacking its BH3-like domain to avoid the induction of apoptosis and facilitate protein isolation. Twenty-four hours after transfection, protein lysates of HeLa cells were subjected to immunoprecipitation using anti–E2 tag or anti–myc tag antibody, followed by Western blot analysis with anti–myc tag or anti–E2 tag antibodies, respectively. The samples of total protein extracts (input) not subjected to immunoprecipitation were used as positive controls (Figure 5, B and C). We could efficiently coprecipitate E2-PXT1-BH3del and c-MYC-BAT3 with anti–E2 tag (Figure 5B) or anti–myc tag (Figure 5C) antibody. We did not find any unspecific precipitation of c-MYC-BAT3 protein in lysate of cells transfected with c-MYC-BAT3 vector only using the anti–E2 antibody, although this protein could be detected in input fraction (Figure 5B). In lysates of untransfected cells, which served as specificity controls, no positive signals were detected (Figure 5, B and C). Taken together, our results clearly demonstrate that mouse PXT1 interacts with BAT3.

Determination of the binding regions between PXT1 and BAT3

To characterize the structural requirements of the PXT1-BAT3 association, we generated a set of constructs expressing truncated PXT1 and BAT3 proteins and tested them via direct Y2H assay for

interactions with Bat3pGAD10 (clone no. 100) or Pxt1pGBKT7 (encoding a full-length PXT1) vectors, respectively. For mapping the BAT3-binding site in PXT1 protein sequence, we used four different fragments cloned in pGBKT7 vector, two encoding N-terminal, namely 1a (aa 2–30) and 1b (aa 2–26), as well as two encoding C-terminal, namely 2a (aa 24–51) and 2b (aa 20–51) parts of PXT1 (Figure 5D). Subsequently the direct Y2H experiments, using as a prey Bat3pGAD10 vector (clone no. 100) and as bait pGBKT7 vector containing sequence encoding one of the above-mentioned PXT1 fragments, were performed. The blue yeast colonies growing on –LTHA, +α-gal plates indicated the interaction, whereas the white yeast colonies growing on –LT plates served as positive control of cotransformation. The analysis demonstrated that the site of PXT1-BAT3 interaction was included in 1a, 2a, 2b, but not in the 1b part of PXT1 (Figure 5D). The minimum region of overlap between BAT3-binding fragments of PXT1 was found to be a short motif of Leu-Ala-Pro-Phe (LAPF) at aa position 27–30. To further validate whether this sequence forms a functional core of the interaction motif, we performed an additional direct Y2H assay using as bait a mut-part1aPxt-1pGBKT7 vector encoding a mutated 1a fragment of PXT1 in which LAPF was changed into Gly-Ala-Pro-Ala (GAPA) sequence (Figure 5E). The mutation of leucine into glycine and phenylalanine into alanine within the LAPF motif in 1a fragment of PXT1 prevented its binding to BAT3, thereby confirming its essentiality for this interaction (Figure 5E). The localization of PXT1-binding site in BAT3 was performed according to the same strategy. Yeasts were transformed with the Pxt1pGBKT7 vector (encoding a full-length PXT1) and one of the three different BAT3 fragments cloned into pGADT7 vector. As illustrated in Figure 5F, fragment 1 of BAT3 was equivalent to aa 169–323, fragment 2 located at aa positions 359–761 contained proline- and glutamine-rich regions, and fragment 3 resided at aa positions 756–1119 and included the C-terminal BAG domain. The direct Y2H assays demonstrated that PXT1-binding site in BAT3 overlaps with proline- and glutamine-rich regions in fragment 2 (Figure 5F).

BAT3 inhibits proapoptotic activity of PXT1

To localize the intracellular site of PXT1-BAT3 interaction, we investigated the coexpression patterns of EGFP-PXT1 and BAT3-dsRED fusion proteins in HeLa and NIH3T3 cells. Surprisingly, the colocalization of the fusion proteins was observed in the nucleus of cotransfected HeLa cells (Figure 6, A–D). Nevertheless, it should be noted that, in a few HeLa cells, the colocalization could also be found in both nucleus and cytoplasm (data not shown). The colocalization study in NIH3T3 cells demonstrated the overlapping fluorescence signals in the nuclear and/or cytoplasmic compartments (Supplemental Figure 3). These observations suggest that the nucleus is a main site of interaction between PXT1 and BAT3 and that BAT3 could mediate nuclear import of cytoplasmic PXT1. Interestingly, during this analysis, we noticed that cells coexpressing EGFP-PXT1 and BAT3-dsRED fusion proteins displayed a normal, nonapoptotic morphology (Figure 6A–D). This prompted us to analyze whether PXT1-BAT3 interaction is necessary to decrease the PXT1-induced apoptosis. As described previously, the LAPF sequence of the PXT1 protein is essential for the interaction with BAT3; therefore, a Pxt-1EGFPC1-LAPFmut vector was constructed, which encodes mutated EGFP-PXT1-LAPFmut fusion protein containing Gly-Gly-Gly-Gly (GGGG) motif instead of LAPF sequence. First, HeLa cells were transfected with Pxt1EGFPC1-LAPFmut construct, and the proapoptotic activity of the EGFP-PXT1-LAPFmut fusion protein was analyzed. As presented in Figure 6E, quantification analysis demonstrated that the level of apoptosis in HeLa cells overexpressing EGFP-PXT1-LAPFmut fusion protein is similar to HeLa cells overexpressing EGFP-PXT1 fusion protein (84% ± 4% vs. 77% ± 8%, respectively, P = 0.33). Next we analyzed whether the mutation of LAPF sequence prevents the interaction with BAT3-dsRED fusion protein. HeLa cells were cotransfected with constructs encoding BAT3-dsRED and EGFP-PXT1 or EGFP-PXT1-LAPFmut fusion proteins. The mutation of the LAPF motif significantly reduced the interaction of EGFP-PXT1-LAPFmut with BAT3-dsRED fusion protein as compared with control EGFP-PXT1 fusion protein (43% ± 12% vs. 91% ± 9% cotransfecetd cells demonstrated interaction, respectively, $P < 0.01$). Unexpectedly, the majority of cells expressing BAT3-dsRED and mutated EGFP-PXT1-LAPFmut fusion proteins displayed normal morphology (Figure 6, G–J), similar to cells expressing BAT3-dsRED and not changed EGFP-PXT1 fusion proteins. Quantification of degenerating HeLa cells coexpressing BAT3-dsRED and either EGFP-PXT1 or EGFP-PXT1-LAPFmut demonstrated a significantly reduced level of apoptosis than that observed in cells overexpressing only EGFP-PXT1 (18% ± 2% or 10% ± 7% vs. 77% ± 8%, respectively, $P < 0.01$; Figure 6K). These findings imply that BAT3 might be involved in regulation of PXT1-induced apoptosis, but that the BAT3-PXT1 interaction is not indispensable for this process.

DISCUSSION

The expression of *Pxt1* is restricted to male germ cells and starts at primary spermatocyte stage (Grzmil *et al.,* 2007). To elucidate the role of *Pxt1* in male germ cells, we have generated a transgenic line in which the cMYC-PXT1 fusion protein is expressed under the control of the 1.4-kb region of the human *PGK2* promoter. The *PGK2* promoter is known to drive male germ cell–specific expression (Robinson *et al.,* 1989; Tascou *et al.,* 2001). We demonstrated that overexpression of *Pxt1* strongly induces degeneration of germ cells, subsequently leading to disruption of spermatogenesis and finally male infertility. Although the c-MYC-PXT1 fusion protein colocalized with peroxisomal marker proteins, the peroxisomal function was not impaired as any accumulation of VLCFA or deficiency in plasmalogens was detected in degenerating germ cells. Using the TUNEL and Annexin V assays, we have demonstrated that germ cells of transgenic males and transiently transfected cells (HeLa and NIH3T3) overexpressing PXT1 undergo apoptosis. At the N terminus of PXT1, we identified a putative BH3-like domain and confirmed its importance for the proapoptotic activity of this protein. Moreover, we demonstrated the interaction between PXT1 and known apoptosis regulator BAT3. Interestingly, the cells overexpressing both PXT1 and BAT3 showed a strongly reduced apoptosis rate as compared with PXT1-only overexpressing cells; however, the interaction of PXT1 and BAT3 was not necessary for apoptosis inhibition.

Members of the B cell leukemia/lymphoma-2 (BCL-2) family of proteins are well known regulators of apoptosis (Adams and Cory, 2001; Spierings *et al.,* 2005; Skommer *et al.,* 2007). Based on the composition of BCL-2 homology (BH) domains, this family was divided into three subclasses. One of them consists of proteins containing only the BH3 domain that serve as apoptosis inducer (reviewed in Lomonosova and Chinnadurai, 2008). A Pfam-A (http://www.pfam.sanger.ac.uk/search) search using a hidden Markov model (HMM) (Sonnhammer *et al.,* 1998) revealed that the N-terminal part of mouse PXT1 contains a putative BH3-like sequence, which is highly conserved between mouse, chimpanzee, and human. This sequence follows the consensus of BH3 motif: ΦΣXXΦXXΦΣDZΦΓ, where Φ represents hydrophobic residues, Σ small residues, Z acidic residue, and Γ is a hydrophilic residue (Day *et al.,* 2008). The core of the BH3 domain consisting of LXXXGDE residues (Lanave *et al.,*

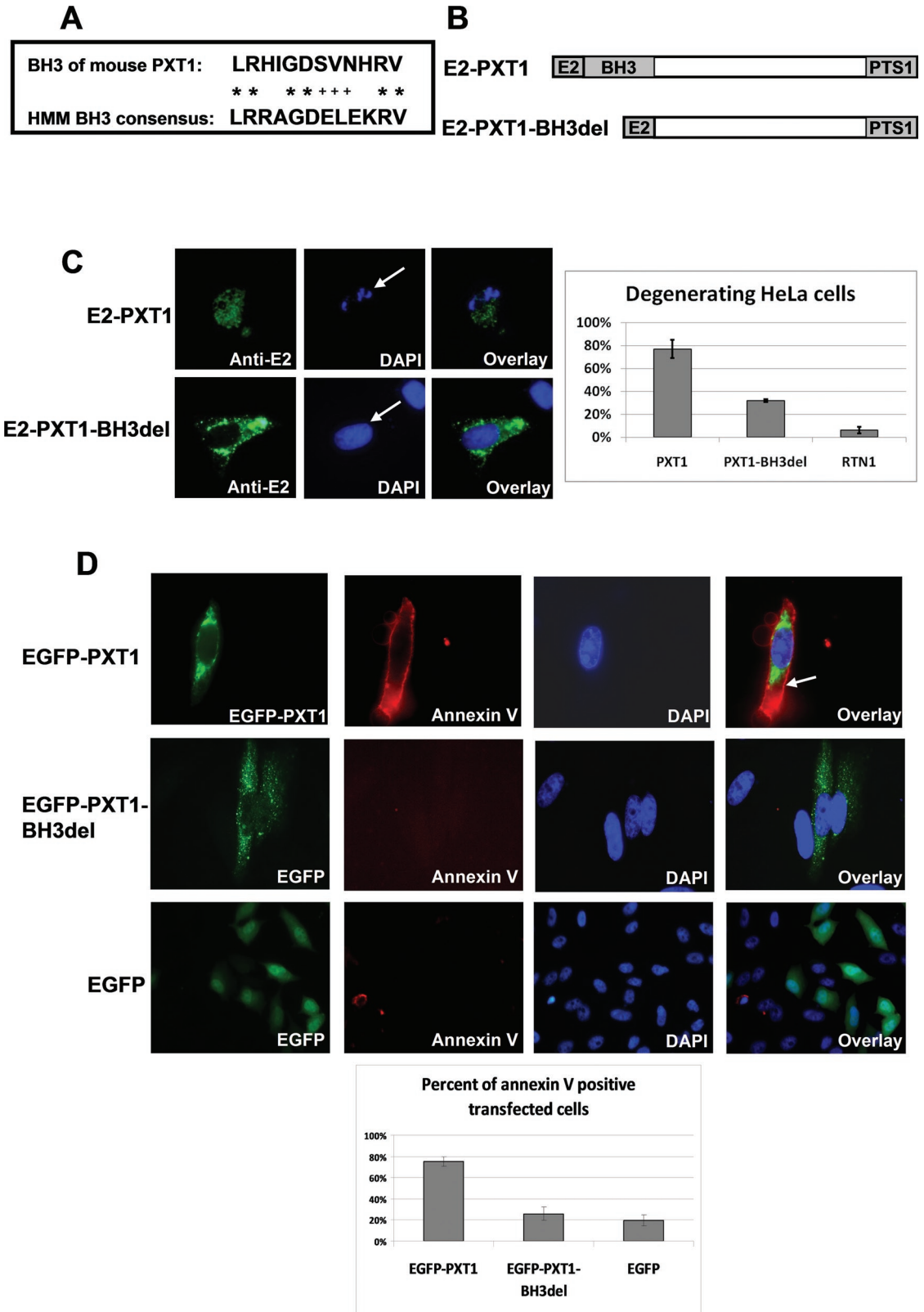

FIGURE 4: The analysis of the BH3-like domain of mouse PXT1. (A) The PFAM database search revealed the presence of BH-like motif at the N terminus of PXT1. (B) To analyze whether the BH3 motif is functional, two constructs were generated. The first construct expresses E2-PXT1 protein containing the complete ORF of PXT1 fused with E2 tag. The second construct encodes E2-PXT1-BH3del, a truncated PXT1 protein lacking the BH3-like domain. (C) The overexpression of PXT1 protein induces cell death in transfected HeLa cells. Using anti–E2 tag antibody, the fusion protein could be detected in the cytoplasm of degenerating cells (top). A total of 77% of all transfected HeLa cells demonstrated evident signs of degenerations. In contrast, the majority of the cells transfected with E2-PXT1-BH3del appeared normal (bottom), and only 32% of them shows signs of degenerated. As a control, cells were transfected with

2004) was also found within the BH3 sequence of PXT1 (LRHIGDS). The only difference is that, in PXT1, instead of the acidic E, the neutral S is present within this sequence. It should be noted that the E residue is not strictly conserved (Lomonosova and Chinnadurai, 2008) and that a variant of BH3 motif with S was also found in human BID protein, which has a proapoptotic function (Tan *et al.,* 1999; Billen *et al.,* 2009).

Conserved leucine (L) and aspartate (D) amino acids of the BH3 core sequence are involved in the interaction and neutralization of anti-apoptotic proteins, thus triggering apoptosis (Hinds and Day, 2005). The overexpression of PXT1 resulted in apoptosis in two transiently transfected cell lines (HeLa and NIH3T3), whereas the deletion of the BH3 domain caused significant reduction of apoptosis rate in transiently transfected cells. However, the decrease in apoptotic cell death did not reach the levels seen in control transfection, suggesting that PXT1 might contain some other domains that could be involved in the apoptotic signaling. The BCL2/adenovirus E1B 19-kDa interacting protein 3 (BNIP3) also contains a BH3 motif and can induce apoptosis in transfected cells. The deletion of the sequence encoding the BH3 domain resulted in significant reduction of cell death; however, the apoptotic rate remained above the value for control transfection (Yasuda *et al.,* 1998). Similar results were also obtained for *Bbc3* (Han *et al.,* 2001) and *Spike* (Mund *et al.,* 2003), indicating that this is a relatively common phenomenon. Since c-MYC-PXT1 fusion protein colocalizes with peroxisomal marker proteins, it could be postulated that the overexpression of PXT1 can impair the cellular peroxisomal import, which can eventually lead to cell death (Maxwell *et al.,* 2003; Jungwirth *et al.,* 2008). No hallmarks of affected peroxisomal function were detected in testes of transgenic animals; thus we can conclude that the BH3 domain of PXT1 protein is functional and responsible for proapoptotic activity.

The signaling pathway controlling the apoptosis events mediated by BCL-2 protein family is essential for proper spermatogenesis (reviewed in Sofikitis *et al.,* 2008). Our transgenic model clearly demonstrates that PXT1 protein is also involved in apoptotic regulation of the cellular homeostasis in the testis. We showed that the overexpression of PXT1 induces apoptosis of male germ cells, mainly spermatocytes. Similar progressive germ cell degeneration was observed in mice with gene-trap mutation of *Bcl2l2* (also known as *Bcl2w*) gene (Ross *et al.,* 1998; Russell *et al.,* 2001). It should be noticed that weak expression of transgenic *c-myc-Pxt1* mRNA was also detected in spermatogonia (in testis at 10 dpp), which with time could result in PXT1 accumulation and SCO phenotype observed in older animals (>103 dpp). In addition to apoptosis in germ cells, the overexpression of PXT1 induced cell death also in transiently transfected HeLa and NIH3T3 cells. Other BH3-only proteins were also demonstrated to induce apoptosis in germ cells and somatic cells; for example, PUMA induces apoptosis in neonatal gonocytes after γ-irradiation (Forand and Bernardino-Sgherri, 2009) and in transfected neuronal and FLS cells (Wyttenbach and Tolkovsky, 2006; You *et al.* 2006). Similarly, the proapototic activity of BIM and BIK was demonstrated to be crucial for spermatogenesis (Coultas *et al.,* 2005; Akhtar *et al.,* 2008), and both proteins induced cell death in transfected somatic cells (Han *et al.,* 1996; Zhang *et al.,* 2006). The molecular mechanism underlying apoptosis induction seems to be universal in different cells. In summary, it can be concluded that PXT1 belongs to the BH3-only protein class of the BCL-2 family.

HLA-B–associated transcript 3 (*Bat3*) was reported to modulate apoptosis through interactions with other apoptotic regulators (Thress *et al.,* 1998; Minami *et al.,* 2007; Desmots *et al.,* 2005, 2008). Using different techniques, we were able to demonstrate that PXT1 specifically interacts with BAT3, a BAG domain–containing protein. The first characterized BAG protein, termed BAG1, was shown to interact with BCL-2 by its BAG domain (Takayama *et al.,* 1995). However, the interaction of BAT3 with PXT1 is not mediated by the BAG domain but involves the part of BAT3 between amino acids 359–761. The same region of BAT3 was reported to interact with BORIS protein (Nguyen *et al.,* 2008), thus strongly supporting the finding that a domain responsible for protein–protein interaction must be present in this region. The proline- and glutamine-rich sequences identified in this part of BAT3 protein might represent a so-called low-complexity region (Wootton and Federhen, 1996) reported to be involved in protein–protein interactions (Wright and Dyson, 1999; Sonnhammer and Wootton, 2001). We also identified the region of PXT1 indispensable for the interaction with BAT3. The database search using the BLAST program (Altschul *et al.,* 1990) revealed that, within the LAPF motif, the L and F amino acids are highly conserved between mouse, human, and chimpanzee. Using direct yeast-two-hybrid system, we could demonstrate indeed the L and F to represent key residues in the LAPF motif. In agreement, the mutation of LAPF motif into GGGG sequence was found to strongly reduce the PXT1-BAT3 interaction in HeLa cells; however, this mutation has not completely abolished this interaction. Taken together, our data suggested that the LAPF motif reflects at least the core of the PXT1 domain that interacts with BAT3.

Full-length BAT3 was reported to function as an anti-apoptotic protein (Wu *et al.,* 2004; Kikukawa *et al.,* 2005). Here we show that coexpression of BAT3 with PXT1 protects cells from PXT1-induced cell death. Moreover, in cells cotransfected with BAT3 and PXT1, the colocalization signals were observed in the nucleus, but this interaction and translocation of PXT1 from cytoplasm to the nucleus is not necessary for the protective role of BAT3. It has been reported that BAT3 can interact with another proapoptotic protein, namely papillomavirus binding factor (PBF) (Sichtig *et al.,* 2007). Likewise, the BAT3-PBF interaction resulted in a significant decrease in PBF-induced cell death (Tsukahara *et al.,* 2009). The authors also demonstrated that, in osteosarcoma cells, PBF-induced apoptosis could be suppressed by nuclear colocalization of PBF and BAT3; however, the cytoplasmic BAT3-PBF interaction in 293EBNA cells could not inhibit the PBF-induced cell death (Tsukahara *et al.,* 2009). Another report demonstrated that the cleaved form of BAT3, lacking the nuclear localization signal, was located in cytoplasm and activated cell rounding, nuclear condensation, and phosphatidylserine exposure (Wu *et al.*, 2004). These findings together with our results suggest that not the interaction per se, but the nuclear localization of overexpressed BAT3 could regulate apoptosis.

Rtn1pQM-Ntag/A vector encoding the RTN1 protein. (D) To validate that degenerating cells indeed undergo apoptosis, the EGFP-PXT1 transfected cells were stained with Annexin V–Alexa 568. The green fluorescence was observed in cells expressing EGFP-PXT1 fusion protein. Cells positive for Annexin V showed red staining. The analysis demonstrated that the plasma membrane of EGFP-PXT1-expressing cells was positive for Annexin V (overlay, white arrow). Cells, transfected with vector encoding for an EGFP-PXT1-BH3del fusion protein without the BH3 domain, demonstrated green fluorescence but very rare also the red staining. The control cells were transfected with EGFP alone. As presented in the diagram, a significant majority of EGFP-PXT1-positive cells showed Annexin V staining (75%) in contrast to EGFP-PXT1-BH3del- or EGFP-transfected cells (26% and 19%, respectively).

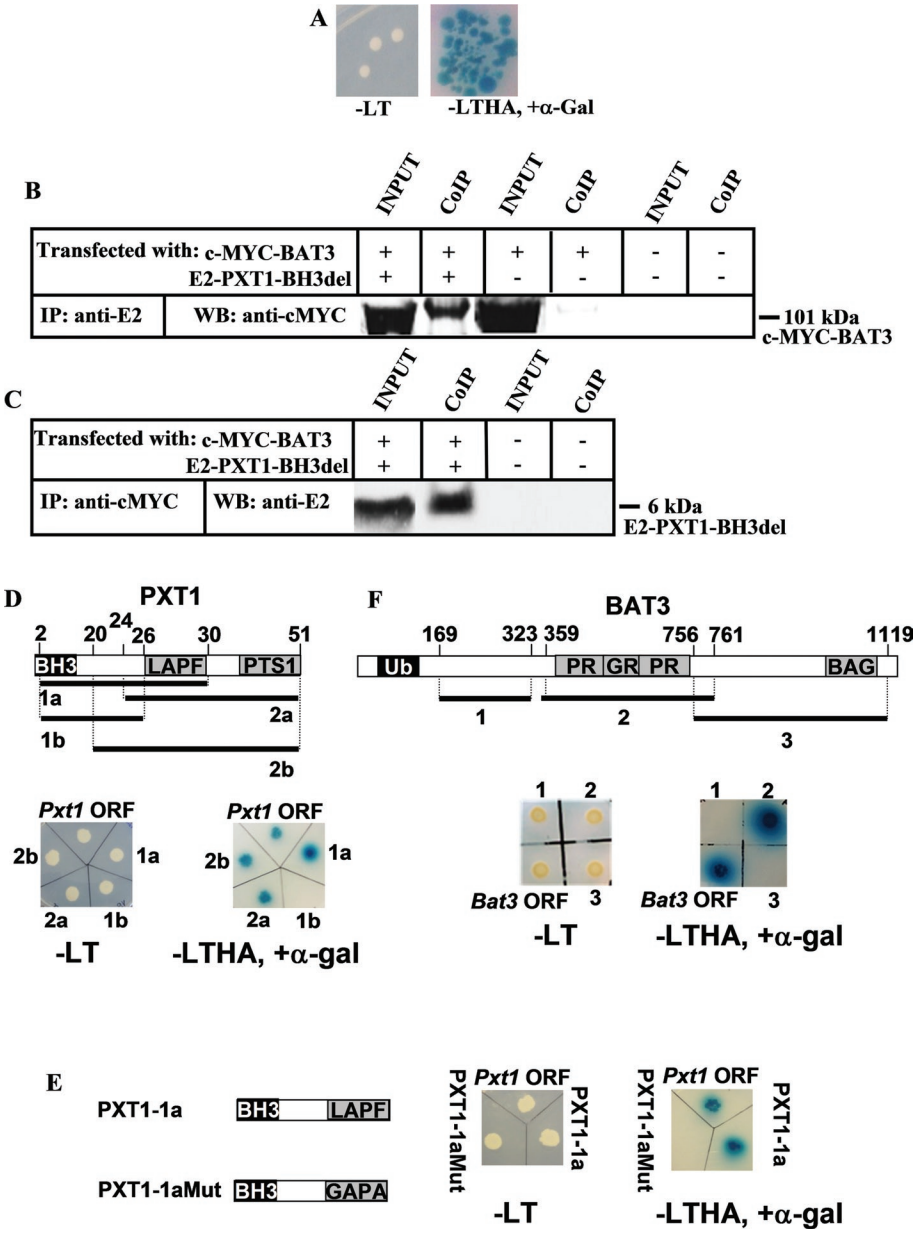

FIGURE 5: The analysis of PXT1-BAT3 interaction. (A) Confirmation of the association between PXT1 and BAT3 via direct Y2H assay using Pxt1pGBKT7 as a bait and Bat3pGAD10 as a prey vector. White yeast colonies growing on nutritional medium lacking leucine and tryptophan (−LT) served as a positive control of cotransformation. Blue yeast colonies growing on medium lacking leucine, tryptophan, histidine, and adenine (−LTHA) but containing X-α-gal (+ α-gal) indicate activation of GAL-4 reporter genes by PXT1-BAT3 interaction. (B) Coimmunoprecipitation of murine PXT1 and BAT3. E2-PXT1-BH3del and c-MYC-BAT3 were coexpressed in HeLa cells. As a control, proteins from single transfection with c-MYC-BAT3 and from untransfected cells were used. Protein extracts were subjected to immunoprecipitation using the anti–E2 antibody. A 5% of the total protein volume was not subjected to immunoprecipitation and used as positive controls (input). Next Western blot analysis using anti–c-myc tag antibody was performed. The 101-kDa band representing the c-MYC-BAT3 fusion protein is clearly visible in proteins from cotrasnsfected cells. In contrast, no signal can be detected in proteins from single transfected cells with c-MYC-BAT3 only, although a strong band is visible in input. Similarly, no unspecific signals were observed in proteins from untransfected cells. (C) The reverse coimmunoprecipitation also demonstrated that E2-PXT1-BH3del fusion protein could be efficiently coprecipitated by anti–c-myc and detected by anti-E2 antibody. Negative control using proteins from untransfected cells confirmed the specificity of the reaction. (D) Schematic view of truncated fragments of PXT1 used for identification of domain responsible for the interaction with BAT3 in direct yeast two-hybrid assay. White colonies growing on –LT plate demonstrated successful cotransformation. Blue colonies growing on –LTHA, +α-gal plates represented the interaction of BAT3 with different parts of PXT1. No growing of yeast expressing BAT3 and part 1b of PXT1, which is lacking the LAPF motif, indicates that this motif is indispensable for the interaction. (E) To check the functionality of the LAPF motif, a mutation was introduced into the part 1a-PXT1 sequence. Although efficient cotransformation was demonstrated on –LT plates, yeast containing BAT3 and part 1a of PXT1 with the GAPA sequence instead of LAPF were not able to grow on –LTHA, +α-gal plates. This result indicates that the LAPF motif is important for PXT1-BAT3 interaction. (F) Schematic representation of truncated fragments of BAT3 generated for identification of the domain involved in interaction with PXT1. Yeast were cotransfected with Pxt1pGBKT7 and one of each parts of Bat3pGADT7. Only part 2 expressing yeast were able to growth on –LTHA, +α-gal plates, indicating that this part contains the domain responsible for the interaction with PXT1. Efficient cotransformation was demonstrated on –LT plates. BH3, BH3-like domain; PTS1, peroxisomal targeting signal type 1; Ub, ubiquitin-like domain; BAG, BCL-2-associated athanogene domain; PR/GR, proline-, glutamine-rich, respectively.

The expression of *Bat3* was reported to be the strongest in the testis (Wang and Liew, 1994; Desmots *et al.*, 2005). In mutants with targeted disruption of *Bat3*, the first changes of testicular histology were observed at 14 dpp, the phenotype became more severe at 42 dpp with increased apoptosis events. The degeneration of germ cells was progressive with only few spermatocytes and no spermatids observed at 140 dpp (Sasaki *et al.*, 2008). The similarity in phenotype of both *Bat3*$^{-/-}$ and the PXT1 transgenic line indicates that the PXT1-BAT3 interaction could be important in the regulation of spermatogenesis. We suggest that, in PXT1-overexpressing males, the balance in concentration of both proteins is disturbed; thus endogenous BAT3 expression might not be sufficient to preserve normal spermatogenesis.

Peroxisomes are responsible for different metabolic pathways, including plasmalogen synthesis (Brites *et al.*, 2003). In the testis, plasmalogens protect germ cells from the negative effect of VLCFA, and the disruption of plasmalogen synthesis leads to germ cell degeneration and apoptosis (Brites *et al.*, 2009). The importance of peroxisomal fatty acid metabolism was also demonstrated in Sertoli cells (Huyghe *et al.*, 2006a, 2006b). However, until now, almost nothing has been known about the role of peroxisomal proteins in controlling apoptosis. A rare exception represents the

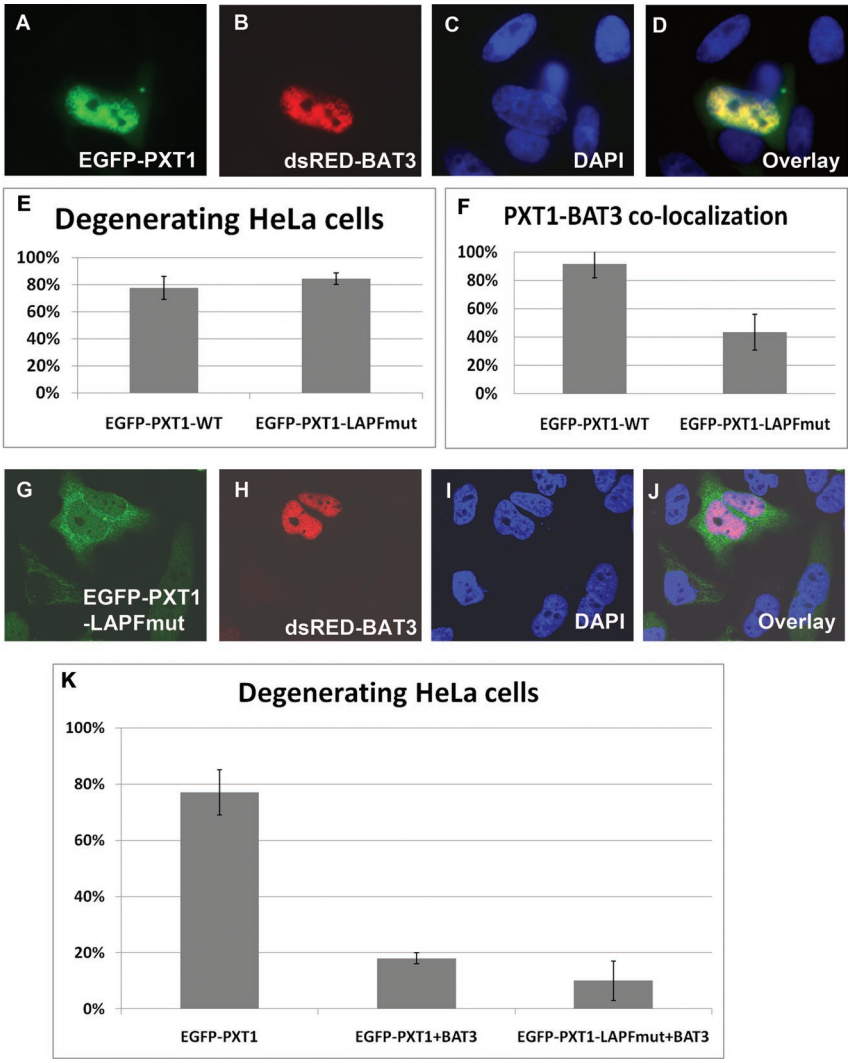

FIGURE 6: BAT3 translocates PXT1 to the nucleus and protects cells from PXT1-induced apoptosis. HeLa cells were transiently cotransfected with Pxt1EGFPC1 and Bat3DsRed vectors. (A) Green fluorescence was observed for EGFP-PXT1, whereas (B) red fluorescence indicates BAT3-dsRED fusion proteins. (C) Nuclei were counterstained with DAPI and display normal nonapoptotic morphology. (D) Green-red overlay (yellow) is clearly visible in the nucleus of cotransfected cells and represents the colocalization of both fusion proteins. To analyze whether the PXT1-BAT3 interaction and translocation of PXT1 to the nucleus is necessary for the anti-apoptotic activity of BAT3, the LAPF motif of PXT1 was mutated into the GGGG sequence. (E) HeLa cells expressing EGFP-PXT1-LAPFmut fusion protein demonstrated the same apoptotic ratio as cells expressing not changed EGFP-PXT1 fusion protein. (F) The mutation of the LAPF motif significantly reduced the interaction of EGFP-PXT1-LAPFmut with BAT3-dsRED fusion protein. In the majority of cotransfecetd cells, green signal representing EGFP-PXT1-LAPFmut was observed in the cytoplasm (G), whereas red fluorescence of BAT3-dsRED fusion protein was detected in the nucleus (H). Nuclei were counterstained with DAPI (I), and no overlay of green-red signals can be observed (J), indicating that both fusion proteins did not colocalize. (K) The quantification analysis showed that the level of apoptosis in HeLa cells coexpressing EGFP-PXT1 or EGFP-PXT1-LAPFmut and BAT3-dsRED fusion proteins is approximately three- to fourfold lower than that observed in EGFP-PXT1-only-expressing cells. The experiments demonstrate that PXT1-induced apoptosis is repressed by overexpression of BAT3, but the PXT1-BAT3 interaction is not indispensable for this activity.

fission 1 (mitochondrial outer membrane) homologue (*Fis1*) gene, which is localized in both the outer mitochondrial membrane and peroxisomes (Koch *et al.*, 2005). RNAi-mediated *Fis1* depletion affected cell sensitivity to apoptosis (Lee *et al.*, 2004). Nevertheless, to our knowledge, no peroxisomal protein was reported to act as a proapoptotic factor. The function of PXT1 in inducing apoptosis suggests that peroxisomes in male germ cells are involved in programmed cell death, indicating a new function of this important cellular compartment.

MATERIALS AND METHODS

Animals

All animals were housed in the Animal Facility of the Institute of Human Genetics (Göttingen, Germany) under controlled environmental conditions (21°C, 12-h light/12-h dark cycle) with free access to standard mouse chow and tap water. All of the experimental procedures were carried out in accordance with the local ethics commission under license number 33.11.42502–04-096/07.

Generation of the c-myc-Pxt1 transgenic mice

The c-myc–Pxt1 transgenic construct contains the following: promoter region of human phosphoglycerate kinase 2 (*PGK2*), c-myc tags, the complete open reading frame (ORF) of murine *Pxt1*, 3′ untranslated region (UTR) of human growth hormone 1 (*GH1*), and SV40 poly(A) sequence. The transgenic cassette was generated according to Tascou *et al.* (2001) with pBluescript II SK (+/−) vector (Stratagene, La Jolla, CA) containing a 1.4-kb region of *PGK2* promoter flanked by *Xho*I/*Hin*dIII restriction sites. The 351-bp *Eco*RI/*Not*I fragment, including leader sequence and five copies of c-myc tag, was amplified by PCR using pCS2–3′mt plasmid (Rupp *et al.*, 1994) as a template, C-mycTag-new-F, Ad.C-mycTag-R primers and cloned downstream of the *PGK2* promoter. All primer sequences are given in Supplemental File 1. The 179-bp *Not*I/*Sac*II *Pxt1* coding sequence was amplified by RT-PCR with mouse testis cDNA and adPxt1-ORF-F, adPxt1-ORF-R primers and cloned downstream of the c-myc tag. In this reaction, two glycine residues were introduced between the fragment consisting of c-myc tags and the *Pxt1* ORF to facilitate proper and independent folding of this two components in c-MYC-PXT1 fusion protein. The 161-bp 3′ UTR of human *GH1* was obtained after PCR on human genomic DNA using hGH-3UTRsacII-F and hGH-3UTRsacII-R primers and afterward was cloned downstream of the *Pxt1* ORF. The 128-bp SacII/SacI fragment containing SV40 poly(A) was amplified by PCR using pEGFP-N1 vector (Clontech, Mountain View, CA) as a template and ad.polA-SV40-F, ad.polA-SV40-R primers. Finally, the SV40 polyadenylation signal was included at the 3′ end of the transgenic construct. After sequencing, the obtained 2.3-kb transgenic cassette was excised from pBluescript II SK (+/−) vector by *Xho*I/*Sac*I digestion and then purified from agarose gel (QIAquick Gel Extraction Kit; Qiagen, Valencia, CA). Subsequently the construct was diluted to a concentration of 30 μg/ml in TE buffer (5 mM Tris, pH 7.4, and 0.1 mM EDTA, pH 8.0) and microinjected into the pronuclei of fertilized

oocytes of the FVB/N strain of mice as described (Hogan *et al.*, 1986). Founder transgenic mice were identified by standard PCR on genomic DNA using gen_hPGK2_F1 and gen_Pxt1ex.2–3_R primers. The quality of genomic DNA was verified by PCR with transition protein 2 (*Tnp2*)-specific primers: TP2_F1 and TP2_R1.

Generation of expression constructs

The primer sequences and the cloning strategies for generation of the expression constructs used in this work are given in Supplemental File 2. The following constructs were generated: Pxt1pQM-Ntag/A, encodes the E2-PXT1 fusion protein; Pxt1ΔBH3pQM-Ntag/A, encodes the E2-PXT1-BH3del mutant fusion protein lacking the BH3-like domain of PXT1; Rtn1pQM-Ntag/A, expresses the E2-RTN1 as described previously (Mannan *et al.*, 2006); Bat3p-CMV contains *Bat3* cDNA (exons 7-25) fused with c-myc tag and encodes the c-MYC-BAT3 fusion protein; Pxt1EGFPC1, encodes EGFP-PXT1 fusion protein as previously described (Grzmil *et al.*, 2007); Pxt1EGFPC1-BH3del, encodes EGFP-PXT1-BH3del mutant fusion protein lacking the BH3-like domain of PXT1; PXT1C1-LAPF-mut, encodes the EGFP-PXT1 fusion protein in which mutation of LAPF motif into GGGG sequence was introduced; Bat3DsRed, contains *Bat3* cDNA (exons 7-25) fused with dsRED and encodes the BAT3-dsRED fusion protein; Pxt1pGBKT7 contains the complete ORF of *Pxt1*; part1a/part1b Pxt1pGBKT7, express the N-terminal parts of PXT1; part2a/part2b Pxt1pGBKT7, express the C-terminal parts of PXT1; mut-part1aPxt1pGBKT7 vector, encodes the N-terminal part of PXT1 in which mutation of LAPF motif into GAPA sequence was introduced; part1Bat3pGADT7 contains mouse *Bat3* cDNA "part 1" located between exon 6 and 9; part2Bat3pGADT7 contains "part 2" of mouse *Bat3* cDNA overlapping exons 9–15; and part3Bat3pGADT7 contains "part 3" of mouse *Bat3* cDNA located between exons 15 and 24.

Cell culture, transfection, immunocytochemistry, and apoptotic cell death assay

Human cervical adenocarcinoma (HeLa) and mouse embryonic fibroblast (NIH3T3) cells were maintained in DMEM supplemented with 10% fetal calf serum and 1% penicillin/streptomycin (PAN-Biotech, Aidenbach, Germany), and in case of NIH3T3 cells, with 1× nonessential amino acids (Life Technologies, Darmstadt, Germany) in a humidified atmosphere of 5% CO_2 at 37°C.

Transfection was performed, as described (Grzmil *et al.*, 2007; Kaczmarek *et al.*, 2009), with 1 μg (for single transfection) or 2 × 0.5 μg (for cotransfection) of construct(s) DNA. After 24 h of transient transfection, the cells were fixed with 4% paraformaldehyde and 0.1% Tween 20 for 15 min at RT. Cells expressing EGFP and/or dsRED fluorescence proteins were mounted with Vectashield mounting medium with DAPI (Vector Laboratories, Burlingame, CA) and proceeded to fluorescence microscopic analysis. The cells transfected with Pxt1pQM-Ntag/A, Pxt1ΔBH3pQM-Ntag/A, or Rtn1pQM-Ntag/A vectors were further washed with Dulbecco's phosphate buffered saline (DPBS), permeabilized 15 min in 0.1% Triton X-100/DPBS, and blocked for 1 h at RT in 5% bovine serum albumin (BSA)/DPBS. In the next step, the cells were incubated for 2 h at RT with mouse monoclonal anti-E2 tag antibody (1:500; Abcam, Cambridge, MA) in 1% BSA/DPBS. Subsequently the cells were washed with DPBS and incubated for 2 h at RT with FITC-conjugated anti–mouse IgG secondary antibody (Sigma-Aldrich, St. Louis, MO) diluted to 1:200 in 1% BSA/DPBS. Finally, the cells were washed with DPBS, mounted with Vectashield mounting medium with DAPI, and observed under a fluorescence microscope. Quantification of apoptosis was performed by analysis of nuclear morphology after DAPI staining. The cells displaying the nuclear morphology typical for apoptosis (half-moon-shaped nucleus, DNA condensation, and fragmentation) were related to the total number of positively stained cells by four different investigators. Each investigator performed 2-4 independent transfections and counted every transfection two times with a minimum of 60 cells. Data are presented as percent of apoptotic cells ± SD. Detection of apoptosis by monitoring of phosphatidylserine translocation in plasma membrane was performed on HeLa cells 24 h after transfection with Pxt1EGFPC1, Pxt1EGFPC1-BH3del, or empty EGFPC1 vector. HeLa cells were washed twice with incubation buffer (10 mM HEPES/NaOH, pH 7.4, 140 mM NaCl, 5 mM $CaCl_2$) and then subjected to combined Annexin V–Alexa 568 (Roche, Mannheim, Germany) and DAPI (Vector Laboratories, Burlingame, CA) labeling for 15 min at RT in the absence of light. Immediately after staining, cells were analyzed under a fluorescence microscope (Olympus BX60).

RT-PCR and Northern blot analysis

Total RNA was isolated from different adult mouse tissues and from testes of transgenic animals at 10, 15, 17, and 19 dpp using the peqGOLD TriFast reagent (Peqlab, Erlangen, Germany) according to the manufacturer's recommendations. For RT-PCR, 2 μg of RNA was treated with DNase-I (Sigma, Munich, Germany) and reverse transcribed using Superscript II reverse transcriptase system and the Oligo $dT_{(12–18)}$ primer (Invitrogen, Darmstadt, Germany). As a control, the same reaction without reverse transcriptase was prepared simultaneously. Subsequently an aliquot of cDNA (1 μl) was subjected to 35 cycles of PCR with Taq DNA polymerase (Immolase; Bioline, Luckenwalde, Germany). Finally, to confirm the reaction specificity, PCR products were isolated and sequenced. Expression of mouse *Pxt1* was determined using Pxt1-ORF-EcoRI-F and Pxt1-ORF-BamHI-R primers yielding a 175-bp-long PCR product. C-myc-Pxt1 transgene expression was detected by RT-PCR with Q-PCR_cmyc_F and Q-PCR_Pxt1ex2–3_R primers generating a 121-bp-long product specific for transgenic transcript. The cDNA quality was verified with mHPRT-For-Q and mHPRT-Rev-Q primers amplifying a 222-bp fragment of the mouse *Hprt1* gene (GeneID: 15452). For Northern blot analysis, 20 μg of total RNA was size fractionated by electrophoresis, transferred onto Hybond XL membrane (Amersham, Freiburg, Germany), and hybridized with a ^{32}P-labeled probe. Mouse *Pxt1*-specific probe was generated by RT-PCR using Pxt1-ORF-*Eco*RI-F and Pxt1-ORF-*Bam*HI-R primers. *Eco*RI/*Not*I fragment of the transgenic construct was used as *c-myc* tag–specific probe. After hybridization, blots were washed at medium to high stringency, and radioactive signals were detected on x-ray film. The RNA quality was verified by rehybridization with a ^{32}P-labeled mouse *Eef1a1* cDNA (GeneID: 13627) probe, generated by PCR using Eef1a1F1 and Eef1a1R1 primers. The *Eef1a1* probe was kindly provided by R. Hahnewald.

Protein extraction, immunoprecipitation, and Western blot analyses

Total proteins from mouse tissues were prepared from the organic phase obtained after RNA isolation using peqGOLD TriFast reagent (Peqlab, Erlangen, Germany) according to the TriReagent protein extraction protocol (Molecular Research Center, Cincinnati, OH), but the protein pellet in 1% SDS was additionally sonicated on ice (Branson Sonifier 250). For immunoprecipitation experiments, proteins were isolated from transiently transfected HeLa cells and precipitated with appropriate antibodies (mouse monoclonal anti–E2 tag or rabbit polyclonal anti–myc tag, 1:100; Abcam) as described (Rzymski *et al.*, 2008). For Western blot analysis, protein samples

were separated on 4–12% or 12% NuPAGE Novex Bis-Tris gel (Invitrogen) and electroblotted onto PVDF membranes (0.45-µm Hybond-P PVDF [Amersham Biosciences] or 0.2-µm PVDF [Invitrogen]). After blocking in 5% nonfat milk TBST (137 mM NaCl, 10 mM Tris-HCl, pH 7.3, 0.1% Tween 20) for 1 h at RT, the membrane was probed overnight at 4°C with the following primary antibodies: mouse monoclonal anti–myc tag (1:2000; Millipore, Temecula, CA), rabbit polyclonal anti–c-myc (1:1500; Sigma-Aldrich, St. Louis, MO), mouse monoclonal anti–E2 tag (1:1000; Abcam, Cambridge, MA), and mouse monoclonal anti–β-actin (1:10,000; Abcam, Cambridge, MA). Subsequently blots were washed three times for 10 min in 2% nonfat milk TBST and incubated for 1–2 h with alkaline phosphatase–conjugated anti–mouse/rabbit IgG secondary antibody (1:5000; Sigma-Aldrich, St. Louis, MO). Finally, blots were washed again and signals were visualized using the BCIP-NBT system (Roth, Karlsruhe, Germany) according to the manufacturer's instruction.

Immunofluorescence assay

Testes of transgenic and wild-type mice were fixed in Bouin's solution and embedded in paraffin. For immunofluorescence analysis, 0.5-µm-thick sections were boiled for 5 min (two times) in 10 mM sodium citrate, pH 6.0, in a microwave. Subsequently sections were incubated for 1 h at RT in blocking buffer (2% normal sheep serum, 0.5% Triton X-100 in DPBS). Next the sections were hybridized overnight at 4°C with following primary antibodies diluted in blocking buffer: mouse monoclonal anti–myc tag (Millipore; diluted 1:100), rabbit polyclonal anti–PMP70 (Abcam; 1:500), rabbit polyclonal anti–Catalase (Abcam; 1:200), and rabbit polyclonal anti–PEX13 antibody (Sigma; 1:200). Afterward, slides were washed in DPBS and incubated for 1 h at RT with Cy3-conjugated anti–mouse and FITC-conjugated anti–rabbit IgG secondary antibodies (Sigma-Aldrich) diluted to 1:500 in blocking buffer. Finally, the slides were washed three times with DPBS, air dried, and mounted with Vectashield medium containing DAPI (Vector Laboratories). The slides were observed under a fluorescence microscope (BX-60, Olympus).

Biochemical plasmalogen and VLCFA analyses

Individual testes (ca. 50 mg each) from adult wild-type and transgenic mice were disintegrated mechanically and dried under a nitrogen stream. VLCFA were derivatized with acetylchloride as methylesters and determined by GC/MS calibrated with internal deuterated standards following a method of Hunneman and Hanefeld (1988). Plasmalogens were determined following a published method (Duran and Wanders, 2008), and levels were expressed relatively to C16:0 and C18:0. VLCFA and plasmalogens were analyzed on a GC/MS (Agilent Technologies, Santa Clara, CA; 8690N/5975B) equipped with a HP-5MS column (Agilent Technologies).

Histological analysis and TUNEL assay

Histological and TUNEL analyses were performed as previously described (Burnicka-Turek *et al.*, 2009). Briefly, for morphological examination, 5-µm-thick paraffin sections of Bouin fixed testes and epididymes were stained with hematoxylin and eosin (Sigma Aldrich). For analysis of apoptosis, deparaffinized and rehydrated sections were subjected to TUNEL assay after pretreatment with proteinase K (Roche Diagnostics) using an ApopTag peroxidase in situ apoptosis detection kit (Qbiogene, Heidelberg, Germany) according to the manufacturer's instruction. Within testis cross-sections, apoptosis was quantified by counting the number of TUNEL-positive and TUNEL-negative tubules per section and TUNEL-positive cells in each tubule. Data are presented as average number of TUNEL-positive cells per tubuli ± SD. For each animal 10–15 fields were counted, at least 2 animals were used for each group. Slides were analyzed under a light microscope (BX-60, Olympus).

Yeast two-hybrid screen (Y2H)

To identify putative PXT1 interacting proteins, a mouse testis cDNA library, constructed in pGAD10 vector (Clontech, Heidelberg, Germany) and kindly provided by I. Adham, was screened with mouse PXT1. The bait construct Pxt1pGBKT7 encoding a GAL4 DNA-binding domain fused with PXT1 was generated as described above. After auto-activation test of the Pxt1pGBKT7 vector, the testis cDNA library screening was performed by the sequential transformation according to Matchmaker GAL4 Two-Hybrid System 3 & Libraries user manual (Clontech). The yeasts were initially spread on medium-stringency plates (SD/−LTH), and then the surviving colonies were verified on high-stringency plates (SD/−LTHA + X-α-Gal). Next plasmid DNA was isolated from blue colonies using Yeastmaker Yeast Plasmid Isolation Kit (Clontech). Subsequently the plasmid DNA was transformed into *E. coli* DH5alpha competent cells (Invitrogen), and clones containing only the prey-library plasmid were selected on LB/Amp and LB/Kan plates. The cDNA inserts of these clones were amplified by PCR with 5′D-LD-insert and 3′AD-LD-insert primers and then sequenced. To confirm PXT1-BAT3 interaction determined by library screen, direct reconstruction of Y2H experiment was performed. In this assay, the identified Bat3pGAD10 prey vector and the Pxt-1pGBKT7 bait construct were cotransformed into AH109 yeast strain by the lithium acetate method according to the Clontech protocol. The cotransformants were selected on SD/−LT plates and the interaction was finally verified on SD/−LTHA + X-α-Gal plates. The same method was used for mapping of PXT1 and BAT3 regions essential for the interaction. All bait and prey vectors used in the study were verified for host yeast toxicity and autonomous activation of reporter genes.

Statistical analysis

For statistical analysis, data obtained by counting apoptotic cells were pooled for each cell type and vector used. Likewise, the data collected after TUNEL analyses were pooled for each genotype and age group. The results were expressed as a ratio; thus they were normalized by angular transformation prior to the t-test for independent groups. Data of plasmalogens and VLCFA analysis (C16:0, C18:0, and C22:0) followed the normal distribution therefore the *t*-test for independent group was applied. In contrast, C24:0 and C26:0 measurement results were not normally distributed nor could be normalized by any kind of transformation. Therefore, the non-parametric alternative for *t*-test, the Mann–Whitney *U* test was used. A P value below 0.05 was considered statistically significant. All statistical analyses were performed using the Statistica 8 software package (StatSoft, Tulsa, OK).

ACKNOWLEDGMENTS

We thank U. Fuenfschilling and S. Thiel for assistance with the generation and breeding of transgenic mice. We are grateful to E. Niedzialkowska and R. Kumar for their help in counting apoptotic cells, O. Shancer for help with preparation of BAT3-dsRED construct, R. Hahnewald for the *Eef1a1* probe, and I. Adham for providing the testis cDNA library. We also thank A. Herwig and J. Mänz for technical assistance, I. Paprotta for help in performing the TUNEL assay, N. Putzer for preparing paraffin sections, and S. Wolf for excellent animal care.

REFERENCES

Adams JM, Cory S (2001). Life-or-death decisions by the Bcl-2 protein family. Trends Biochem Sci 26, 61–66.

Akhtar RS, Klocke BJ, Strasser A, Roth KA (2008). Loss of BH3-only protein Bim inhibits apoptosis of hemopoietic cells in the fetal liver and male germ cells but not neuronal cells in bcl-x-deficient mice. J Histochem Cytochem 56, 921–927.

Altschul SF, Gish W, Miller W, Myers EW, Lipman DJ (1990). Basic local alignment search tool. J Mol Biol 215, 403–410.

Baes M, Huyghe S, Carmeliet P, Declercq PE, Collen D, Mannaerts GP, Van Veldhoven PP (2000). Inactivation of the peroxisomal multifunctional protein-2 in mice impedes the degradation of not only 2-methyl-branched fatty acids and bile acid intermediates but also of very long chain fatty acids. J Biol Chem 275, 16329–16336.

Banerji J, Sands J, Strominger JL, Spies T (1990). A gene pair from the human major histocompatibility complex encodes large proline-rich proteins with multiple repeated motifs and a single ubiquitin-like domain. Proc Natl Acad Sci USA 87, 2374–2378.

Billen LP, Shamas-Din A, Andrews DW (2009). Bid: a Bax-like BH3 protein. Oncogene 27 (Suppl 1), 93–104.

Brites P *et al.* (2003). Impaired neuronal migration and endochondral ossification in Pex7 knockout mice: a model for rhizomelic chondrodysplasia punctata. Hum Mol Genet 12, 2255–2267.

Brites P, Mooyer PA, El, Mrabet L, Waterham HR, Wanders RJ (2009). Plasmalogens participate in very-long-chain fatty acid-induced pathology. Brain 132, 482–492.

Burnicka-Turek O, Shirneshan K, Paprotta I, Grzmil P, Meinhardt A, Engel W, Adham IM (2009). Inactivation of insulin-like factor 6 disrupts the progression of spermatogenesis at late meiotic prophase. Endocrinology 150, 4348–4357.

Casciola-Rosen L, Rosen A, Petri M, Schlissel M (1996). Surface blebs on apoptotic cells are sites of enhanced procoagulant activity: implications for coagulation events and antigenic spread in systemic lupus erythematosus. Proc Natl Acad Sci USA 93, 1624–1629.

Coultas L, Bouillet P, Loveland KL, Meachem S, Perlman H, Adams JM, Strasser A (2005). Concomitant loss of proapoptotic BH3-only Bcl-2 antagonists Bik and Bim arrests spermatogenesis. EMBO J 24, 3963–3973.

Day CL, Smits C, Fan FC, Lee EF, Fairlie WD, Hinds MG (2008). Structure of the BH3 domains from the p53-inducible BH3-only proteins Noxa and Puma in complex with Mcl-1. J Mol Biol 380, 958–971.

Desmots F, Russell HR, Lee Y, Boyd K, McKinnon PJ (2005). The reaper-binding protein scythe modulates apoptosis and proliferation during mammalian development. Mol Cell Biol 25, 10329–10337.

Desmots F, Russell HR, Michel D, McKinnon PJ (2008). Scythe regulates apoptosis-inducing factor stability during endoplasmic reticulum stress-induced apoptosis. J Biol Chem 283, 3264–3271.

Duran M, Wanders RJA (2008). Plasmalogens and polyunsaturated fatty acids. In: Laboratory Guide to the Methods in Biochemical Genetics, ed. N. Blau, M. Duran, and K. M. Gibson, Berlin: Springer Verlag, 207–220.

Fan CY *et al.* (1996). Hepatocellular and hepatic peroxisomal alterations in mice with a disrupted peroxisomal fatty acyl-coenzyme A oxidase gene. J Biol Chem 271, 24698–24710.

Forand A, Bernardino-Sgherri J (2009). A critical role of PUMA in maintenance of genomic integrity of murine spermatogonial stem cell precursors after genotoxic stress. Cell Res 19, 1018–1030.

Grzmil P, Burfeind C, Preuss T, Dixkens C, Wolf S, Engel W, Burfeind P (2007). The putative peroxisomal gene Pxt1 is exclusively expressed in the testis. Cytogenet. Genome Res 119, 74–82.

Han J, Flemington C, Houghton AB, Gu Z, Zambetti GP, Lutz RJ, Zhu L, Chittenden T (2001). Expression of bbc3, a pro-apoptotic BH3-only gene, is regulated by diverse cell death and survival signals. Proc Natl Acad Sci USA 98, 11318–11323.

Han J, Sabbatini P, White E (1996). Induction of apoptosis by human Nbk/Bik, a BH3-containing protein that interacts with E1B 19K. Mol Cell Biol 16, 5857–5864.

Hikim APS, Wang C, Lue Y, Johnson L, Wang XH, Swerdloff RS (1998). Spontaneous germ cell apoptosis in humans: evidence for ethnic differences in susceptibility of germ cell death. J Clin Endocrinol Metab 83, 152–156.

Hinds MG, Day CL (2005). Regulation of apoptosis: uncovering the binding determinants. Curr Opin Struct Biol 15, 690–699.

Hogan B, Constantini F, Lacy E (1986). Manipulating the Mouse Embryo. A Laboratory Manual, Cold Spring Harbor, NY: Cold Spring Harbor Laboratory, 151–205.

Hunneman DH, Hanefeld F (1988). Diagnose von peroxisomalen Erkrankungen–Erfahrungen mit einer empfindlichen massenfragmentographischen Bestimmung der sehr langkettigen Fettsäuren und der Phytansäure im Plasma. Monatsschrift Kinderheilkunde 136, 529.

Huyghe S, Mannaerts GP, Baes M, Van Veldhoven PP (2006b). Peroxisomal multifunctional protein-2: the enzyme, the patients and the knockout mouse model. Biochim Biophys Acta 1761, 973–994.

Huyghe S, Schmalbruch H, De Gendt K, Verhoeven G, Guillou F, Van Veldhoven PP, Baes M (2006a). Peroxisomal multifunctional protein 2 is essential for lipid homeostasis in Sertoli cells and male fertility in mice. Endocrinology 147, 2228–2236.

Jungwirth H, Ring J, Mayer T, Schauer A, Büttner S, Eisenberg T, Carmona-Gutierrez D, Kuchler K, Madeo F (2008). Loss of peroxisome function triggers necrosis. FEBS Lett 582, 2882–2886.

Kaczmarek K, Niedzialkowska E, Studencka M, Schulz Y, Grzmil P (2009). Ccdc33 a predominantly testis expressed gene encodes a putative peroxisomal protein. Cytogenet Genome Res 126, 243–252.

Kikukawa Y, Minami R, Shimada M, Kobayashi M, Tanaka K, Yokosawa H, Kawahara H (2005). Unique proteasome subunit Xrpn10c is a specific receptor for the antiapoptotic ubiquitin-like protein Scythe. FEBS J 272, 6373–6386.

Koch A, Yoon Y, Bonekamp NA, McNiven MA, Schrader M (2005). A role for Fis1 in both mitochondrial and peroxisomal fission in mammalian cells. Mol Biol Cell 16, 5077–5086.

Lanave C, Santamaria M, Saccone C (2004). Comparative genomics: the evolutionary history of the Bcl-2 family. Gene 333, 71–79.

Lee YJ, Jeong SY, Karbowski M, Smith CL, Youle RJ (2004). Roles of the mammalian mitochondrial fission and fusion mediators Fis1, Drp1, and Opa1 in apoptosis. Mol Biol Cell 15, 5001–5011.

Lomonosova E, Chinnadurai G (2008). BH3-only proteins in apoptosis and beyond: an overview. Oncogene 27 (Suppl 1), S2–S19.

Luers GH, Schad A, Fahimi HD, Volkl A, Seitz J (2003). Expression of peroxisomal proteins provides clear evidence for the presence of peroxisomes in the male germ cell line GC1spg. Cytogenet Genome Res 103, 360–365.

Luers GH, Thiele S, Schad A, Volkl A, Yokota S, Seitz J (2006). Peroxisomes are present in murine spermatogonia and disappear during the course of spermatogenesis. Histochem Cell Biol 125, 693–703.

Manchen ST, Hubberstey AV (2001). Human Scythe contains a functional nuclear localization sequence and remains in the nucleus during staurosporine-induced apoptosis. Biochem Biophys Res Commun 287, 1075–1082.

Mannan AU, Boehm J, Sauter SM, Rauber A, Byrne PC, Neesen J, Engel W (2006). Spastin, the most commonly mutated protein in hereditary spastic paraplegia interacts with Reticulon 1 an endoplasmic reticulum protein. Neurogenetics 7, 93–103.

Maxwell M, Bjorkman J, Nguyen T, Sharp P, Finnie J, Paterson C, Tonks I, Paton BC, Kay GF, Crane DI (2003). Pex13 inactivation in the mouse disrupts peroxisome biogenesis and leads to a Zellweger syndrome phenotype. Mol Cell Biol 23, 5947–5957.

Minami R, Shimada M, Yokosawa H, Kawahara H (2007). Scythe regulates apoptosis through modulating ubiquitin-mediated proteolysis of the Xenopus elongation factor XEF1AO. Biochem J 405, 495–501.

Mund T, Gewies A, Schoenfeld N, Bauer MK, Grimm S (2003). Spike, a novel BH3-only protein, regulates apoptosis at the endoplasmic reticulum. FASEB J 17, 696–698.

Nenicu A, Luers GH, Kovacs W, David M, Zimmer A, Bergmann M, Baumgart-Vogt E (2007). Peroxisomes in human and mouse testis: differential expression of peroxisomal proteins in germ cells and distinct somatic cell types of the testis. Biol Reprod 77, 1060–1072.

Nguyen P, Bar-Sela G, Sun L, Bisht KS, Cui H, Kohn E, Feinberg AP, Gius D (2008). BAT3 and SET1A form a complex with CTCFL/BORIS to modulate H3K4 histone dimethylation and gene expression. Mol Cell Biol 28, 6720–6729.

Nozawa K, Fritzler MJ, Takasaki Y, Wood MR, Chan EK (2009). Co-clustering of Golgi complex and other cytoplasmic organelles to crescentic region of half-moon nuclei during apoptosis. Cell Biol Int 33, 148–157.

Ozaki T, Hanaoka E, Naka M, Nakagawara A, Sakiyama S (1999). Cloning and characterization of rat BAT3 cDNA. DNA Cell Biol 18, 503–12.

Pogge von Strandmann E *et al.* (2007). Human leukocyte antigen-B-associated transcript 3 is released from tumor cells and engages the NKp30 receptor on natural killer cells. Immunity 27, 965–974.

Robinson MO, McCarrey JR, Simon MI (1989). Transcriptional regulatory regions of testis-specific PGK2 defined in transgenic mice. Proc Natl Acad Sci USA 86, 8437–8441.

Rodemer C, Thai TP, Brugger B, Kaercher T, Werner H, Nave KA, Wieland F, Gorgas K, Just WW (2003). Inactivation of ether lipid biosynthesis causes

male infertility, defects in eye development and optic nerve hypoplasia in mice. Hum Mol Genet 12, 1881–1895.
Ross AJ, Waymire KG, Moss JE, Parlow AF, Skinner MK, Russell LD, MacGregor GR (1998). Testicular degeneration in Bclw-deficient mice. Nat Genet 18, 251–256.
Rupp RA, Snider L, Weintraub H (1994). Xenopus embryos regulate the nuclear localization of XMyoD. Genes Dev 8, 1311–1323.
Russell LD, Warren J, Debeljuk L, Richardson LL, Mahar PL, Waymire KG, Amy SP, Ross AJ, MacGregor GR (2001). Spermatogenesis in Bclw-deficient mice. Biol Reprod 65, 318–332.
Rzymski T, Grzmil P, Meinhardt A, Wolf S, Burfeind P (2008). PHF5A represents a bridge protein between splicing proteins and ATP-dependent helicases and is differentially expressed during mouse spermatogenesis. Cytogenet Genome Res 121, 232–244.
Sasaki T, Gan EC, Wakeham A, Kornbluth S, Mak TW, Okada H (2007). HLA-B-associated transcript 3 (Bat3)/Scythe is essential for p300-mediated acetylation of p53. Genes Dev 21, 848–861.
Sasaki T, Marcon E, McQuire T, Arai Y, Moens PB, Okada H (2008). Bat3 deficiency accelerates the degradation of Hsp70–2/HspA2 during spermatogenesis. J Cell Biol 182, 449–458.
Sichtig N, Silling S, Steger G (2007). Papillomavirus binding factor (PBF)-mediated inhibition of cell growth is regulated by 14–3-3beta. Arch Biochem Biophys 464, 90–99.
Silver LM (1995). Mouse Genetics, Oxford, UK: Oxford University Press (http://www.informatics.jax.org/silver/).
Skommer J, Wlodkowic D, Deptala A (2007). Larger than life: mitochondria and the Bcl-2 family. Leuk Res 31, 277–286.
Sofikitis N, Giotitsas N, Tsounapi P, Baltogiannis D, Giannakis D, Pardalidis N (2008). Hormonal regulation of spermatogenesis and spermiogenesis. J Steroid Biochem Mol Biol 109, 323–330.
Sonnhammer EL, Wootton JC (2001). Integrated graphical analysis of protein sequence features predicted from sequence composition. Proteins 45, 262–273.
Sonnhammer EL, von Heijne G, Krogh A (1998). A hidden Markov model for predicting transmembrane helices in protein sequences. Proc Int Conf Intell Syst Mol Biol 6, 175–182.
Spierings D, McStay G, Saleh M, Bender C, Chipuk J, Maurer U, Green DR (2005). Connected to death: the (unexpurgated) mitochondrial pathway of apoptosis. Science 310, 66–67.
Takayama S, Sato T, Krajewski S, Kochel K, Irie S, Millan JA, Reed JC (1995). Cloning and functional analysis of BAG-1: a novel Bcl-2-binding protein with anti-cell death activity. Cell 80, 279–284.
Tan KO, Tan KM, Yu VC (1999). A novel BH3-like domain in BID is required for intramolecular interaction and autoinhibition of pro-apoptotic activity. J Biol Chem 274, 23687–23690.
Tascou S, Nayernia K, Meinhardt A, Schweyer S, Engel W, Trappe R, Burfeind P (2001). Targeted expression of SV40 large tumour antigen (TAg) induces a transient enhancement of spermatocyte proliferation and apoptosis. Mol Hum Reprod 7, 1123–1131.
Thress K, Henzel W, Shillinglaw W, Kornbluth S (1998). Scythe: a novel reaper-binding apoptotic regulator. EMBO J 17, 6135–6143.
Tsukahara T, Kimura S, Ichimiya S, Torigoe T, Kawaguchi S, Wada T, Yamashita T, Sato N (2009). Scythe/BAT3 regulates apoptotic cell death induced by papillomavirus binding factor in human osteosarcoma. Cancer Sci 100, 47–53.
Wang R, Liew CC (1994). The human BAT3 ortholog in rodents is predominantly and developmentally expressed in testis. Mol Cell Biochem 136, 49–57.
Wootton JC, Federhen S (1996). Analysis of compositionally biased regions in sequence databases. Methods Enzymol 266, 554–571.
Wright PE, Dyson HJ (1999). Intrinsically unstructured proteins: re-assessing the protein structure-function paradigm. J Mol Biol 293, 321–331.
Wu YH, Shih SF, Lin JY (2004). Ricin triggers apoptotic morphological changes through caspase-3 cleavage of BAT3. J Biol Chem 279, 19264–19275.
Wyttenbach A, Tolkovsky AM (2006). The BH3-only protein Puma is both necessary and sufficient for neuronal apoptosis induced by DNA damage in sympathetic neurons. J Neurochem 96, 1213–1226.
Yasuda M, Theodorakis P, Subramanian T, Chinnadurai G (1998). Adenovirus E1B-19K/BCL-2 interacting protein BNIP3 contains a BH3 domain and a mitochondrial targeting sequence. J Biol Chem 273, 12415–12421.
You X, Boyle DL, Hammaker D, Firestein GS (2006). PUMA-mediated apoptosis in fibroblast-like synoviocytes does not require p53. Arthritis Res Ther 8, R157.
Zhang J, Chen J, Liu L, Ji C, Gu S, Ying K, Mao Y (2006). Different gene expression profiles of AD293 and HEK293 cell lines that show contrasting susceptibility to apoptosis induced by overexpression of Bim L. Acta Biochim Pol 53, 525–530.